

EASOT-AP: An open-source MATLAB package to estimate the seismic moment, rupture radius, and stress-drop of earthquakes from time-dependent P-wave displacements

Sahar Nazeri^{*}, Aldo Zollo

Department of Physics E. Pancini, University of Naples Federico II, Naples, Italy

ARTICLE INFO

Keywords:

Open-source MATLAB code
Signal processing
Earthquake source
P-wave displacement
Time domain technique

ABSTRACT

We developed a MATLAB package, to rapidly obtain the apparent EArthquake SOurce time function using the Average of near-source P-wave displacement records (EASOT-AP) and to estimate the source parameters of the seismic moment, the rupture radius, and the average static stress drop. The algorithm implemented in this package is based on a rapid and straightforward methodology that is recently developed by Zollo et al. (2021). To this purpose, EASOT-AP models a LPDT curve, which is the average P-wave displacement versus time in the logarithm scale. In this paper, the performance of the EASOT-AP has been shown by evaluating the strong motion data recorded in the near-source range of small magnitude events ($2 = M_w \leq 3$) that occurred in the Irpinia region, southern Italy. The source parameters follow a self-similar, constant-stress-drop scaling with a relatively low average stress drop of about 0.1–0.2 MPa. This Tool is designed for an easy use, and all steps of data processing are performed completely within the numerical environment of MATLAB.

1. Introduction

In the seismological community, a major part of the available knowledge about the nature of the earthquake primarily relies on the analysis and modelling of seismic records. Parallel to the technological novelties in seismic instrument development and the notable improvements in the digital signal processing, many algorithms and methods have been developed to study the physics of earthquake fractures. Normally in worldwide seismological laboratories, after the occurrence of the event, efficient computing workflows are implemented on the seismic datasets to immediately calculate the earthquake location, size, and fault mechanism. Investigating the other features needs a longer time and process like computing the complete kinematic and dynamic earthquake rupture parameters. In addition to the complexity of the rupture process by itself, the seismic waves are ordinarily attenuated and contaminated with multi-path and site effects. So, the application of advanced signal processing and more fast and straightforward methods play an important role in better and rapidly estimating the source parameters.

To estimate the earthquake source parameters, usually, the frequency-domain methods are preferred to be used by seismologists. For instance, the seismic moment of the event is simply derived from the

low-frequency far-field displacement spectrum, independent of the details of the rupture process and type of dislocation on the fault plane. However, the spectral techniques have some remarkable drawbacks. One difficulty refers to the exact estimation of the corner frequency (f_c) which strongly affect the accurate calculation of the stress drop since it depends on the cube of f_c . To have a more precise estimation of f_c with considerable uncertainty, some pre-processing analyses should be accounted like removing the seismic attenuation, path effects, etc. Moreover, choosing the proper time window to perform the analysis in the frequency domain is the other critical issue that determines the appropriate frequency interval to implement the spectral techniques.

On the other hand, determination of the earthquake source parameters in the time domain seems more straightforward despite its less frequent usage. In fact, the main concern is about correctly removing the anelastic attenuation and path effect from the seismograms. More recently, simultaneous with the development of earthquake early warning systems, time-domain strategies have been also proposed to provide an estimate of the kinematic rupture parameters (Colombelli et al., 2014; Nazeri et al., 2019; Wang et al., 2021; Zollo et al., 2021). In this work, we propose a time-domain and parametric method to rapidly determine the main features of the earthquake source using the P-wave signals recorded very close to the radiating source (for example within

* Corresponding author.

E-mail address: sahar.nazeri@unina.it (S. Nazeri).

100 km for large magnitude events, $M > 5.5$). The basic principle of this technique is to model the time evolution of the logarithm of P-wave displacement (P_d) corrected to hypocentral distance (called LPDT curve with an exponential-rise shape) as a proxy of the apparent source time function (STF) of the earthquake (Zollo et al., 2021). Assuming a circular and uniform velocity rupture, the isosceles triangular STF is assumed as a possible model of seismic source retrieved by the far-field P-wave radiated by a point-source. Then without assuming a specific kinematic model, the seismic moment, the rupture dimension, and the average static stress drop are estimated directly from the observation. To generate the LPDT curve, only all available P-wave displacement signals recorded in a pre-defined near-source distance is used. This approach has been tested for a wide range of moderate to large events occurred at different regions so far such as, Japan, Italy, and China, and several papers have been published since 2014 (Colombelli et al., 2014; Nazeri et al., 2019; Wang et al., 2021; Zollo et al., 2021). In this paper we present a MATLAB package (EASOt-AP) to implement this parametric technique based on the latest modification of Zollo et al. (2021). The package contains fast processes, and it is straightforward, simple data entry, user-friendly software, and able to integrate with other systems. After inserting the required inputs, the package is easy-run and fully automatic. Finally, to illustrate how this open-source MATLAB package works, we used the strong motion data of small magnitude ($2 = M_w \leq 3$) events that recently occurred in Irpinia, southern Italy, one of the main areas of the Central and Southern Apennines chain.

2. Method

Since the pioneering observation of Aki (1966) for the 1964 Niigata earthquake, the seismic moment (M_0) and the average fault displacement are inferred as the equivalent source descriptions. The average far-field displacement signal which corresponds to the displacement at the source could provide the appropriate measure of earthquake size and the seismic moment. Although the permanent static displacement on the Earth' surface is described as the near field term, the far field term represents the dynamic response or transient seismic waves. The far-field displacement both in the time- and the frequency-domains are typically approximated by an isosceles triangular source time function.

The moment magnitude of a point-source rupture at a given distance in a homogeneous, half-space and elastic Earth model is calculated using the far-field P-wave displacement recorded on the vertical seismograms to the Earth' surface:

$$M_0 = \frac{4\pi\rho V_p^3}{F_s R_{\theta\varphi}} R \int u^P(t) dt \quad (1)$$

where ρ is density, V_p is P-wave velocity, F_s is the free surface factor, $R_{\theta\varphi}$ is P-wave radiation pattern coefficient, and R is hypocentral distance. $\int u^P(t) dt$ is the area under the P-wave displacement pulse, obtained from the multiplication of two main features of the generated LPDT curve, i. e., the plateau level ($P_L^* \approx \log(P_D R)$) and the corresponding corner time ($T_c \approx \frac{\bar{T}_D}{2}$) as they present the peak amplitude and half duration (\bar{T}_D) of the apparent STF respectively (Nazeri et al., 2019; Zollo et al., 2021). Following same abbreviation by Zollo et al. (2021), the first factor in equation (1) is a constant value for the studied area, named A'^{-1} , and:

$$R \int u^P(t) dt = R \frac{P_D \bar{T}_D}{2} = \frac{10^{P_L^*} \bar{T}_D}{2} \quad (2)$$

in which, the factor $R P_D$ is P-wave amplitude with hypocenter distance correction (Nazeri et al., 2017). Thus, equation (1) is simplified by:

$$M_0 = A'^{-1} \frac{10^{P_L^*} \bar{T}_D}{2} \quad (3)$$

Then, the source radius of a circular rupture and stress drop are calculated by (Keilis-Borok, 1959; Aki et al., 2002; Zollo et al., 2021):

$$a = \frac{\bar{T}_D}{2} / \left(\frac{1}{V_R} - \frac{2}{\pi V_P} \right) \quad (4)$$

$$\Delta\sigma = \frac{7M_0}{16a^3} = \frac{7A'^{-1} 10^{P_L^*}}{4 \bar{T}_D^2} \left(\frac{1}{V_R} - \frac{2}{\pi V_P} \right)^3 \quad (5)$$

However, in case the stress drop, and rupture velocity are preliminary known and invariant with magnitude, the moment magnitude of the event is estimated by merging equations (3)–(5):

$$M_0 = \left(A'^{-1} 10^{P_L^*} \left(\frac{1}{V_R} - \frac{2}{\pi V_P} \right) \left(\frac{7}{16\Delta\sigma} \right)^{1/3} \right)^{3/2} \quad (6)$$

Therefore, the seismic moment and the moment magnitude are calculated using only the estimated plateau level P_L^* of the LPDT curve.

We recall that the moment magnitude formula, $\log M_0 = 1.5M_w + 9.2$ (M_0 is in Nm), as derived by Hanks and Kanamori (1979), implicitly assumes a self-similar constant stress-drop scaling with $\Delta\sigma = 3$ MPa. For source parameter determination of small and moderate size earthquakes, the rupture velocity is generally assumed from the kinematic rupture models that are adopted to evaluate the rupture size. For circular rupture models, a typical value of $V_R = 0.9 V_s$ (V_s is the shear wave velocity) is used (Brune, 1970; Madariaga, 1976).

Depending on the use of (1) only P_L^* and known stress drop values or (2) both P_L^* and T_c parameters, two approaches are followed to estimate (1) only M_0 / M_w (Approach 1) or (2) three source parameters of $M_0 - M_w$, a and $\Delta\sigma$ (Approach 2).

Approach 1 can be also followed to estimate, for a given active seismic region, the average static stress-drop from a subset of previously recorded earthquakes with variable magnitude, for which the LPDT plateau measurements are available, and the moment magnitude is known from the earthquake bulletin. In this case, the optimal average

stress-drop value can be searched by minimizing the $RMS = \sqrt{\frac{\sum_{i=1}^N \Delta M_i^2}{N}}$ of magnitude residuals $\Delta M_i = M_{\text{bull}}^i - M_{\text{LPDT}}^i$ measured over the available catalogue of N earthquakes. For any successive earthquake, occurring in the same region, a rapid estimation of the seismic moment and moment magnitude can be therefore obtained using equation (9) of Zollo et al. (2021), with the previously determined average stress-drop value and fixed rupture velocity.

3. Description of the software, algorithm, and implementation

The EASOt-AP package is designed using MATLAB (R2021a) supported on both operating Systems of Windows and Linux/Ubuntu, thus it is recommended to run it using the same version or later releases of MATLAB. The core algorithm of the program is presented in Fig. 1. The design philosophy of the package divides it into 3 main parts of input (folder “INPUT”), analysis box (folder “CODES”), and output (folder “OUTPUT”). The following sections enumerate all these parts in more detail.

3.1. Input

This package requires SAC formatted strong motion data with the following needed fields in the header: (1) earthquake location (longitude, latitude, depth) and origin time, (2) station coordinates (longitude, latitude, elevation), (3) P-wave arrival time, stored as “A” field, (4) source-receiver distance in kilometre stored as “DIST” field (automatically calculated by SAC after inserting the earthquake and station locations), (5) magnitude of the event (M_w is preferred) reported by agencies as a piece of pre-information (stored as “MAG” field).

It is expected that a quality check of the waveforms is done before running the package, for instance, whenever manually or automatically picking the P-phase. However, the analysis module is provided with

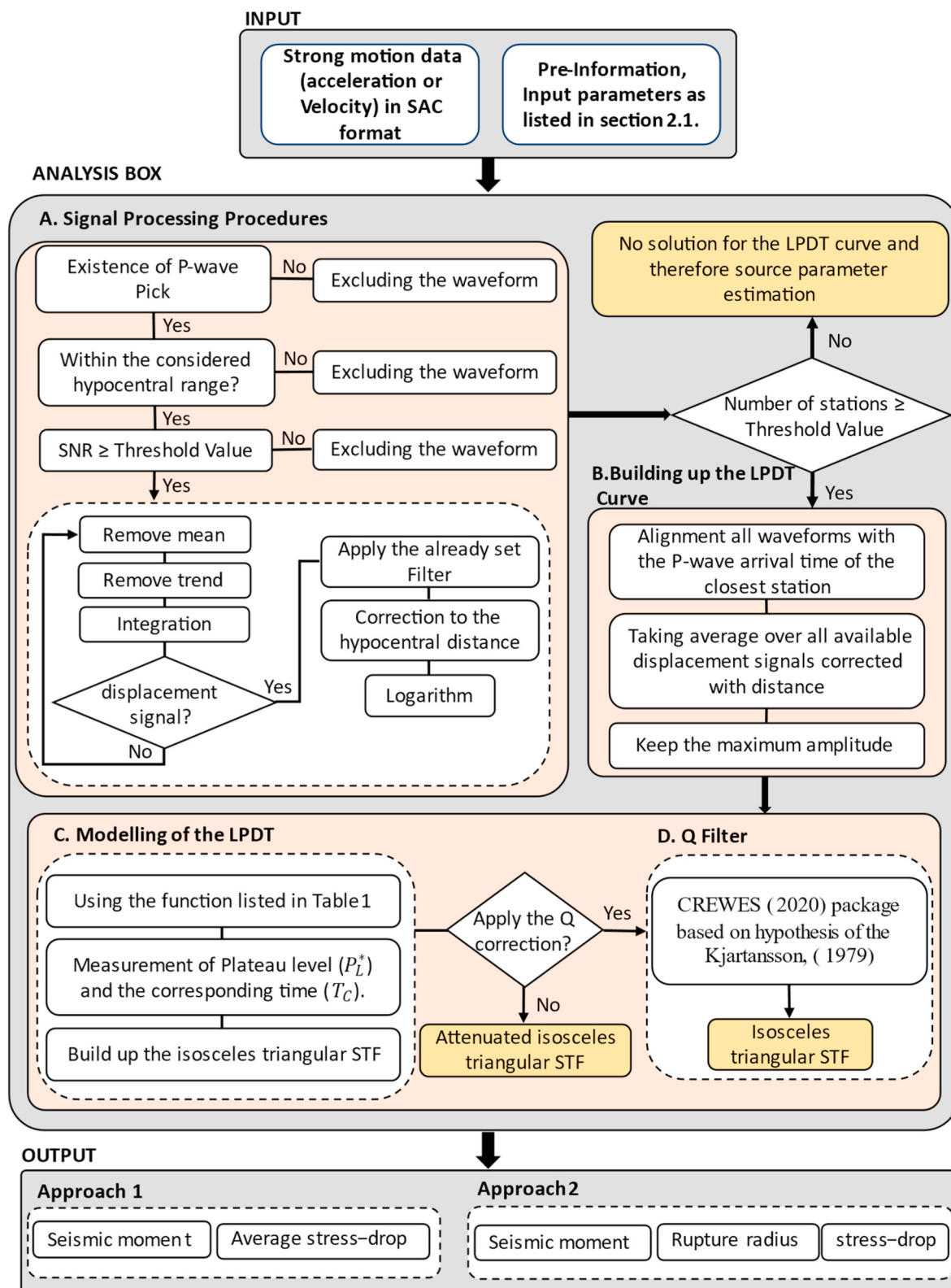


Fig. 1. Sketch map showing flow process of the program LPDT.

checking the quality of data with a signal-to-noise ratio (SNR) larger than a threshold value assigned by the user as an input parameter. Also, it is important to use waveforms with at least 2 s of pre-event signal, otherwise, the waveforms are excluded automatically from the calculation box.

In addition to the strong motion data, the main input file used by

EASOT-AP package is a text file named “Input.txt” saved in the folder of “INPUT”. To increase the flexibility of the data analysis step, this file is provided with a variety of optional parameters/arguments that should be modified for any new analyses or datasets. Description of the set-up of these inputs and their default values are presented in the “Appendix”.

3.2. Analysis box

The core of the EASOT-AP package is the content of the folder of “CODES” that in the following sections, we present a brief description of four main modules including (A) signal processing procedures, (B) building up the LPDT curve, (C) modelling of the LPDT, and (D) optional correction of the anelastic attenuation.

A. Signal processing procedures

This phase starts with reading the vertical seismograms for all stations separately and applying the routines for signal processing procedures including removing mean and trend from data, integration, and applying the chosen filter to the displacement and in case the velocity signals depend on the already set of the parameters/arguments in the input file. To keep high-quality data, one more processing step is applied by excluding the records with an SNR of less than a pre-defined threshold value. SNR is computed in the logarithmic decibel scale using the squared amplitude ratio of the initial part of the P wave and background noise. After this preliminary processing step, the raw data (acceleration or velocity) is converted to displacement signals. As the main idea is to use only the P-wave displacement signals obtained from the vertical component of all available stations within a given hypocentral distance range, the S-wave is excluded considering a constant or variable time window using the S-minus-P coefficient depending on what is already set by the user in the input file.

B. Building up the LPDT curve

To build up the LPDT curve, first, the individual displacement traces are simply corrected to the hypocentral distance to remove the effect of the geometrical spreading for a homogeneous and elastic Earth velocity model (Zollo et al., 2006; Nazeri et al., 2017). Then, all the traces are aligned with reference to the P-onset of the closest station. The next step is looking at a distribution of the series of distance-corrected displacements at each time interval (equivalent to the data sample time) separately from the P-onset to the desired time window to extract the mean/median and 1-standard deviation of the points to create three curves for a given event named as the average ($LPDT_{Average}$), and ± 1 -sigma curves ($LPDT_{\pm SD}$) (Fig. 2). Finally, to smooth the complexity of the curves, the peak amplitude is kept in a progressively expanded

time window, starting from the origin of the LPDT curve ($LPDT_{max}$, red curve in Fig. 2). The LPDT curves have an exponential-rise like shape at the beginning and then continue with a plateau level. It is previously proven (see Fig. 2c, Nazeri et al., 2019) that the critical point of the curve, i.e., the corner time of the plateau level is assumed as the corresponding time of the maximum amplitude of the triangular source time function.

C. Modelling the LPDT curve

A well modelling the observed LPDT curve plays an important role in automatically and correctly extracting the plateau level and corner time. Different authors have recently observed that the use of an exponential function with 2 (Nazeri et al., 2019) or 3 (Wang et al., 2021; Zollo et al., 2021) variable-parameters allows for correct modelling of the curve and reliable estimation of its main features. Fig. 3 clearly shows that in case of any anomalies unlike the expected shape of LPDT curve, the exponential functions (blue curve) fail to well represent the curve in particular in the initial part. While the plateau level is almost a well estimated parameter. This issue is more evident in presence of considerable error of P-wave picking that strongly affects the initial part of the curve, especially for the small magnitude events. So, the alternative solution is a function (called HB) with a similar definition to a High-pass Butterworth filter as it is written in Table 1. As it is obvious in Fig. 3, the HB model (black curve) is well representing the data (red curve) more than the exponential function. Moreover, modeling the LPDT curve using the HB function allows to correct its beginning which is equivalent to the concave (dashed line in Fig. 3, the first critical point of the curve).

To overcome the corner time (T_c) identification problem from the LPDT curves, 2 different strategies have been implemented as explained following:

- (1) Model-driven: time evaluation of the curvature of the fit curve ($f(t)$) to find a time at which curvature tends to zero (magenta diamond, Figs. 2 and 3). Although, parametric representation of curvature is mathematically based on the first and second derivative of a function ($f(t)$); i.e., $\frac{|f''(t)|}{(1+f'(t)^2)^{3/2}}$, here, we use the package “Curvature of a 1D curve in a 2D or 3D space” released on MathWorks (Mjaavatten, 2022). In this package, a curvature of a given point ($f_i(t)$) is calculated as inverse of radius of a circumcentre for every triplet $f_{i-1}(t)$, $f_i(t)$, and $f_{i+1}(t)$ of nearest

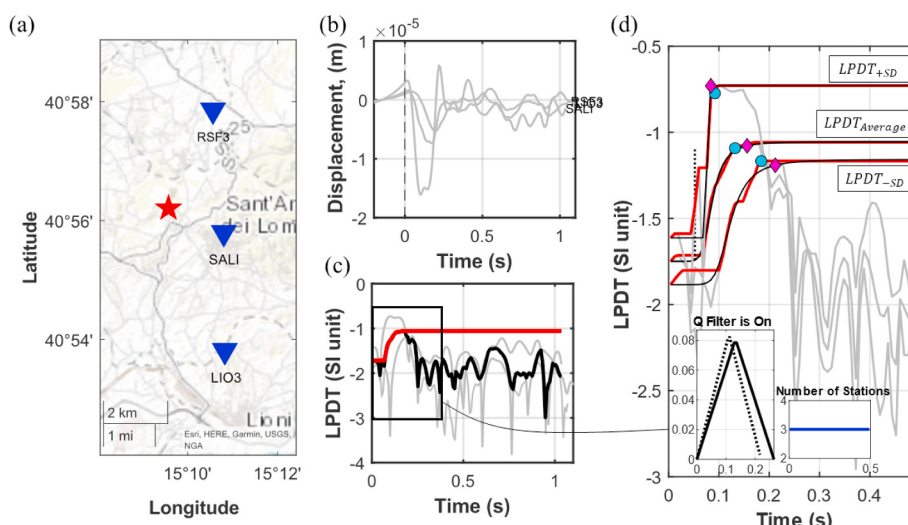


Fig. 2. LPDT curve of a small magnitude event (Mw: 2.9) that occurred in Irpinia, southern Italy with a considerable error in P-wave picking causing a time shift of the LPDT curve. (a) the map shows the geometry of the stations (blue triangles) and epicentre of the event (red star). (b) plot presents the filtered displacement signals. (c) the individual LPDT curve of each station (grey curves), $LPDT_{average}$ (black), and $LPDT_{max}$ (red). (d) the grey and red curves are the $LPDT_{average}$ and $LPDT_{max}$ plus/minus one standard deviation ($LPDT_{\pm SD}$) respectively. The black curves show the best fit to the $LPDT_{max}$ (here HB function is chosen). The dashed black line shows the correct beginning of the LPDT curve. The corner time of the plateau level calculated from model- or data-driven methods is shown with magenta diamond and cyan circle respectively. In a small plot of “Number of Stations”, total number of stations as a function of time, used to build up the LPDT curve, is presented in terms of time. The black triangle shows the source time function (STF) extracted directly from the LPDT curve. While the dotted triangle in the right plot represents the Q-corrected STF. (For interpretation of the references to color in this figure legend, the reader is referred to the Web version of this article.)

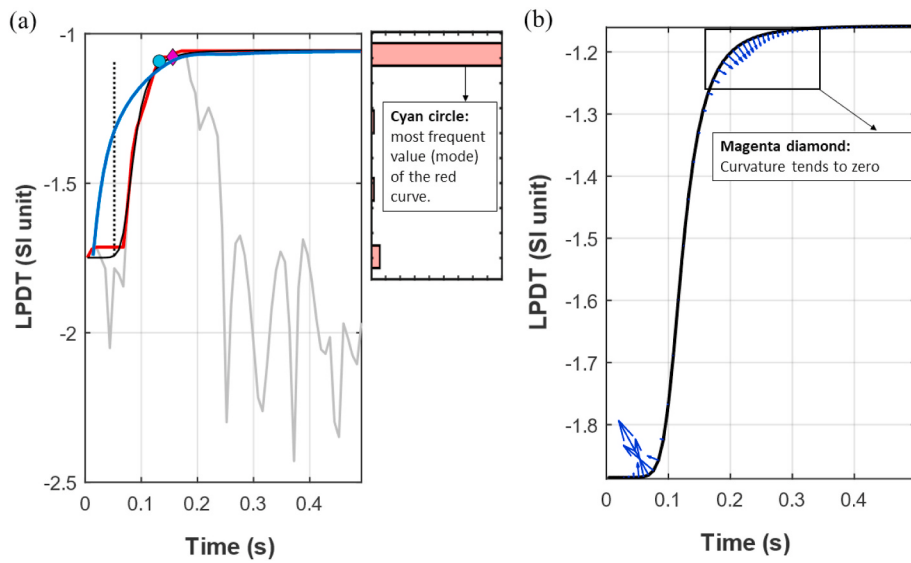


Fig. 3. LPDT curve of one small event as an example to explain how corner time is estimated assuming two different Fit- and Data-driven methods i.e., (a) the mode of the max-curve (histogram), and (b) curvature (arrows) of the fit-curve. The grey and red curve are $LPDT_{average}$, and $LPDT_{max}$ respectively. The blue and black curves show the best fit to the red curve assuming 3-variables exponential and HB functions respectively. The dashed black line shows the corrected beginning of the LPDT curve. (For interpretation of the references to color in this figure legend, the reader is referred to the Web version of this article.)

Table 1

List of the functions, the candidates to model the LPDT curve. In all functions, y_o is the P arrival time-intercept of the curve, while P_L , T_1 , T_2 , T_L , and γ are the fitting parameters estimated by a non-linear multiple variable fitting procedure.

Functions	Variables	Reference
$LPDT(t) = y_o + P_L \left(1 - e^{-\frac{t}{T_L}} \right)$	P_L and T_L	Nazeri et al. (2019)
$LPDT(t) = y_o + P_L \left[1 - 0.5 \left(e^{-\frac{t}{T_1}} + e^{-\frac{t}{T_2}} \right) \right]$	P_L , T_1 and T_2	Zollo et al. (2021)
$LPDT(t) = y_o + P_L \left[1 - \sqrt{\frac{1}{1 + \left(\frac{t}{T_L} \right)^\gamma}} \right]$	P_L , T_L and γ	This study

neighbouring points along the curve. In fact, in this way, the effect of a trade-off between fit parameters becomes less, in addition, to make the codes more independent of the type of function chosen for modelling. Fig. 3 shows an example of time evaluation of the curvature for a given earthquake.

- (2) Data-driven: mode of the $LPDT_{max}$ which presents the most frequent value in which it is equivalent to the maximum of a histogram of the curve (cyan circle, Figs. 2 and 3).

In the end, both values of plateau level and corner time obtained from the curves are used to build up the simplified and attenuated triangular STF as the anelastic attenuation is still not implemented.

D. Q Filter

As previously mentioned, the main assumption of the implemented technique in this package is based on simplifying the source of the earthquake and model configurations of the medium to reduce the attenuation terms affecting the seismic waves. Also, the effect of the local site at the receiver has been ignored. However, the radiated seismic waves are normally attenuated with more factors like heating, reflection, and refraction of the waves from intermediate layers that all are categorized as anelastic attenuation. Losing the energy of the seismic waves is proportional to their amplitude decay and time extension, and it depends differently on the material that is slightly inelastic or elastic. Although the elastic attenuation corresponding to geometrical spreading is removed from the signals by simply correcting the amplitude by distance, to remove the anelastic attenuation effect, a more complex strategy as a deconvolution operator at any station before proceeding

with the computation analysis is required. In the seismology community, the deconvolution operator in a framework of inverse problem theory is a long-established and ill-posed problem in time-domain data processing in the sense that the recovered solution is unstable and very sensitive to the presence of noise in the data.

Here, instead of applying a deconvolution operator on each seismogram separately, the apparent STF obtained from the LPDT curve is corrected at the end. It is done following a global search strategy based on the generation of the synthetic anelastic attenuated triangles at the stations with a known value of the quality factor Q_P . Then, the synthetic LPDT curve and its relevant parameters are computed to be compared with the observed values. For this purpose, the CREWES software for Q modelling (CREWES, 2020) is used in which the linear attenuation model of Kjartansson (1979) is numerically implemented (more detail Zollo et al., 2021).

3.3. Output

The folder “OUTPUT” is automatically deleted and created after each time running the package, and it includes two MATLAB *.mat and Excel *.xlsx format files specified with the name of the region, and two main subfolders of “SignalProcessing”, and “Regression” in case of having more than one event in the selected dataset. The *.mat file stores the “workspace”, while the *.xlsx file includes the earthquake source parameters estimated from the EASOT-AP package following all the above-mentioned approaches in different sheets named “App1”, “App1_FindMinStress”, “App2_Mode”, “App2_QFilter _Mode”, “App2_Curvature”, and “App2_QFilter _Curvature”.

In the folder of “SignalProcessing”, the platform provides two figures for each event. The first figure includes a map showing the location of the event and distribution of stations, displacement signals aligned with the P-arrival time of the closest station in one subplot, and individual LPDT curves plus the $LPDT_{average}$ and $LPDT_{max}$ in the other subplot (two first column in Fig. 2). The second figure shows three LPDT curves: $LPDT_{average}$, and $LPDT_{\pm SD}$ (last column in Fig. 2). Moreover, this folder contains one more figure representing the LPDT curves of all selected earthquakes before and after correcting any time shift of the beginning of the curves (Fig. 4b).

Finally, the directory of “Regression” contains the qualitative output of the package for both approaches, Figs. 6–8.

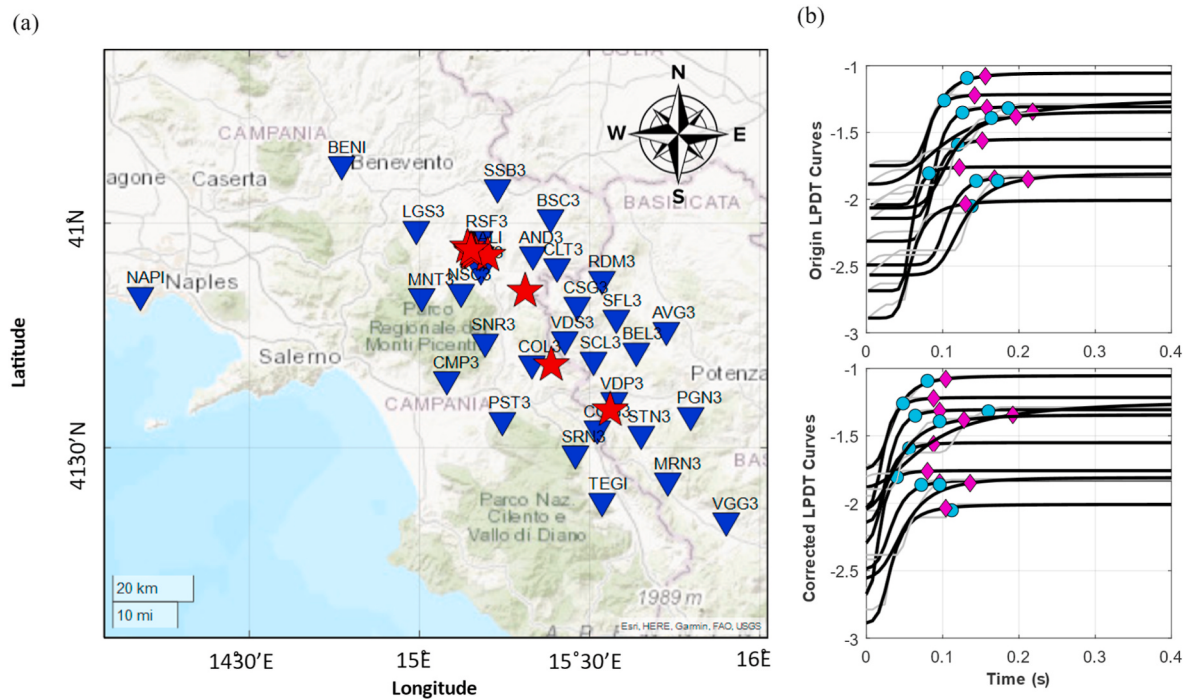


Fig. 4. Application of the package for the few small magnitude events occurred in Irpinia, south Italy, recorded on the ISNet network. **(a)** map of the selected earthquakes, $M < 3$, **(b)** the LPDT curves of the events left: before and right: after correcting the beginning of the curves. The cyan circles and magenta diamonds are data- and fit-driven measurements respectively assumed as a half duration of the STF. (For interpretation of the references to color in this figure legend, the reader is referred to the Web version of this article.)

4. Application to EASOT-AP package

As the package is previously evaluated for moderate to large earthquakes by Zollo et al. (2021), in this section, an application is presented (Figs. 4–8) by analyzing 10 small magnitude events ($M_w > 2$) that occurred in Irpinia, southern Italy, and recorded by the Irpinia Seismic Network (ISNet, the infrastructure of the Irpinia Near-Fault Observatory (INFO)). ISNet is a dense, 6-component, and high-dynamic range seismic network consisting of 31 stations deployed along the Campania-Lucania Apennine chain. The selected data includes the largest events of the 3–7 July 2020 Rocca San Felice sequence that occurred at the northern part of the main segment that ruptured during 1980, November 23, Ms 6.9 Irpinia earthquake (Festa et al., 2021). Fig. 4a shows the location of the ISNet seismic stations and the epicenters used in this study.

The ISNet catalogue includes both local and moment magnitude scales, however, here we used only moment magnitude as a reference to compare with our result. For this application, the LPDT curves (Fig. 4b) are built with at least 3 high-quality vertical components ($\text{SNR} \geq 10$) recorded within a 15 km epicentral distance. Although the available dataset includes both velocity and acceleration waveforms, we used the vertical acceleration records, therefore a 1 Hz high-pass first-order Butterworth filter is only applied to the displacement signals to remove any possible low-frequency effects during the data processing steps.

To launch the procedure on the entire waveform database, parameter tuning is important. For example, choosing the appropriate filter and frequency band is crucial. The EASOT-AP package provides the user with a flexible means of testing various filter options and evaluating their effect on P-wave displacement signals. This filter selection can also be

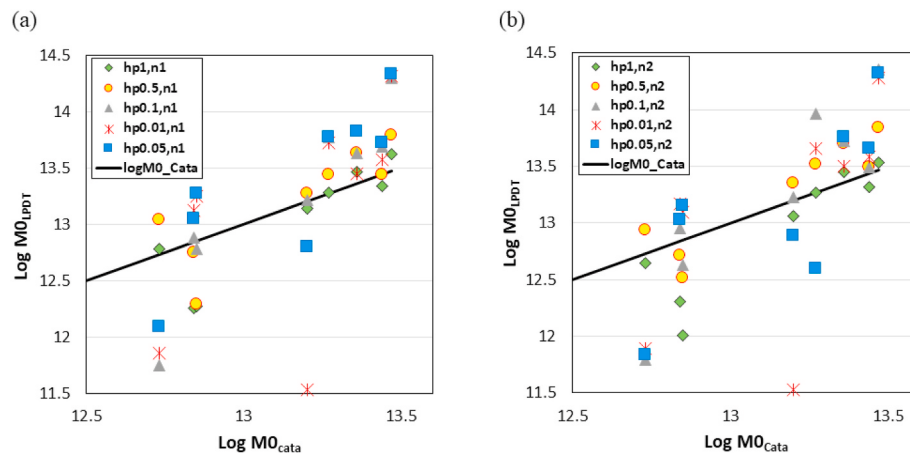


Fig. 5. Effect of the filter on estimation of the seismic moment for few events of the chosen dataset for two number of poles, **(a)** $n = 1$ and **(b)** $n = 2$, and various corner frequency from 0.05 to 1. Comparing to the values reported in the catalogue, our observations assuming the filter with corner frequency of 1 Hz better follows the one-by-one scaling trend (black solid line).

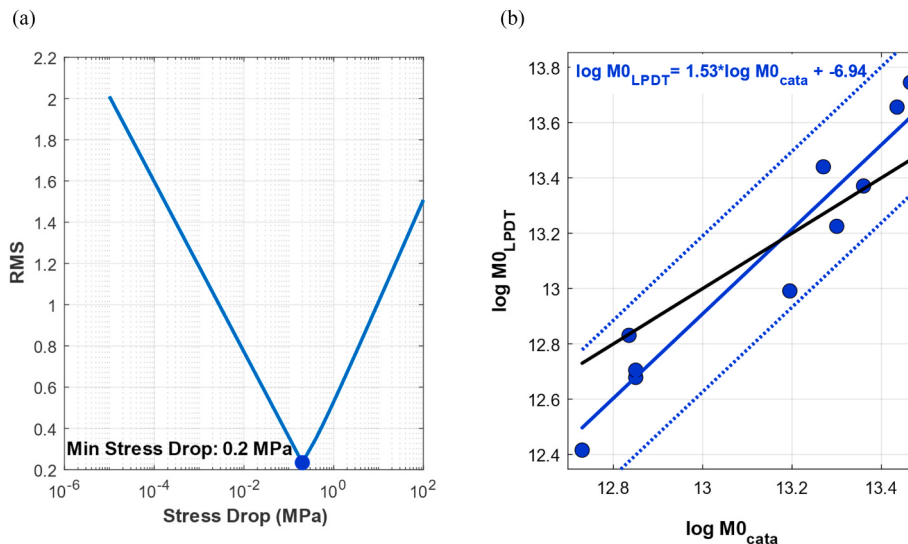


Fig. 6. Approach 1, (a) average stress drop value, i.e., 0.2 MPa calculated from minimizing the magnitude residuals, (b) the logarithm of estimated seismic moment from the LPDT method using the optimum stress drop value, i.e., 0.2 MPa (panel b).

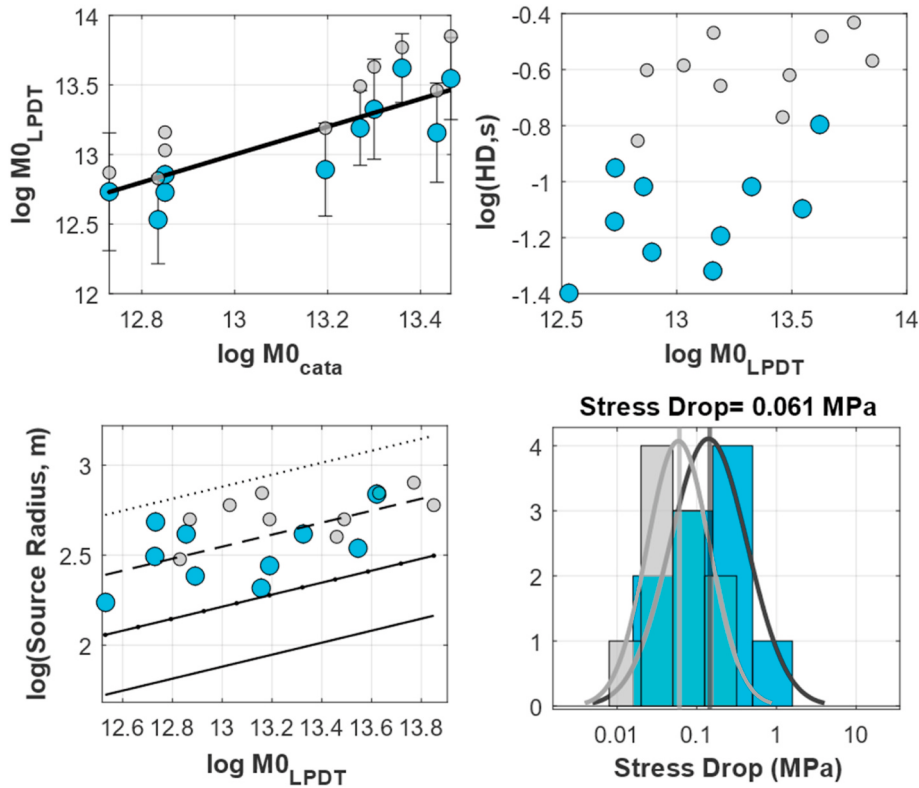


Fig. 7. Approach 2, Data-driven method, the seismic moment, half duration of the STF (HD), source radius, and stress drop before (cyan circle) and after (grey) implementing the anelastic attenuation respectively. (For interpretation of the references to color in this figure legend, the reader is referred to the Web version of this article.)

verified by comparing the estimated source parameters with those reported by agencies and other literature. Figure 5 has been considered for setting the filter for the data used in this study.

The required parameters of the medium i.e., density, P-wave velocity (V_p), V_p -to- V_s ratio, and Q_p are fixed as 2700 kg/m³, 5.5 km/s, 1.7, 220 respectively (Amoroso et al., 2014; Zollo et al., 2014; Festa et al., 2021). The complete result of this application consists of the source parameter estimations and their scaling relation with the magnitude obtained in this study is shown in Figs. 6–8.

The obtained result showed that there is a good consistency between the seismic moment obtained from the LPDT approach with the moment magnitude of the catalogue either after or removing the anelastic attenuation effect shown with grey or colored symbols in the top-left panel of Fig. 6a and b. There is also a good consistency between both data-driven or fit-driven parameters shown with magenta diamond or cyan circle respectively.

The average static stress drop (about 0.1 MPa) is a factor 6 smaller than the value that Festa et al. (2021) obtained for the Rocca San Felice

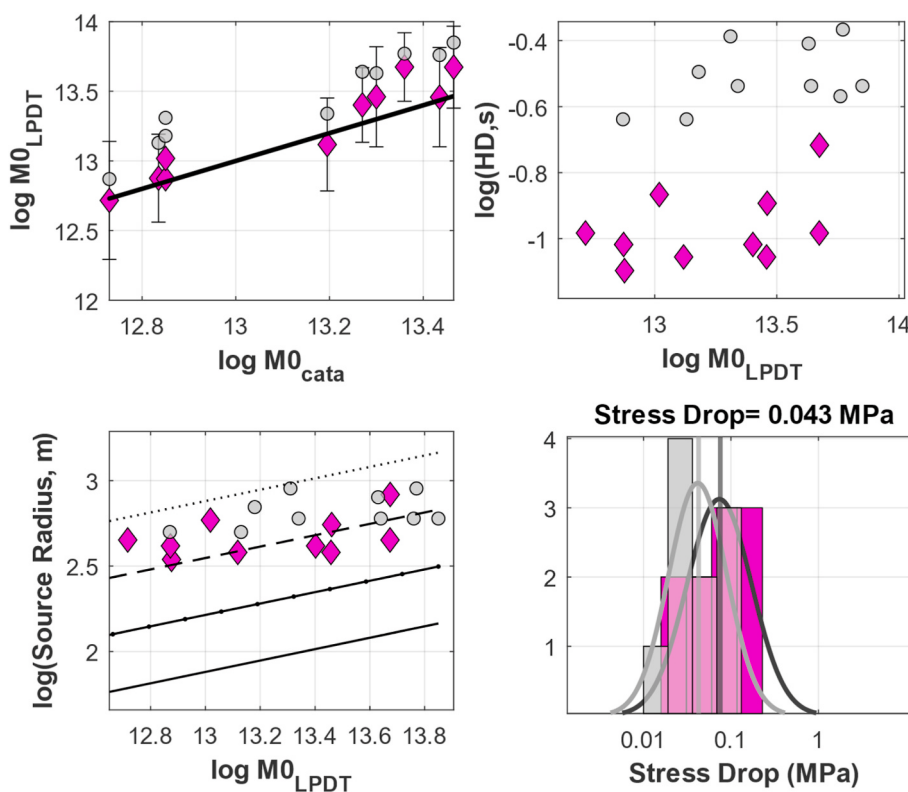


Fig. 8. Approach 2, Model-driven method, the seismic moment, half duration of the STF (HD), source radius, and stress drop before (magenta diamond) and after (grey) implementing the anelastic attenuation respectively.

sequence i.e., 0.64 MPa. Festa et al. (2021), assuming the Brune (1970) source model, calculated the source parameters of the Rocca San Felice sequence in the frequency domain inverting the observed displacement spectra. They interpreted the low stress drop value with the presence of a fluid-driven initiation mechanism of the sequence. Zollo et al. (2014) observed a higher static stress drop of 1.4 MPa for Irpinia, while their apparent stress value of about 0.1 MPa is in the same range as our result. Like Festa et al. (2021), Zollo, et al. (2014) used spectrum techniques to analyze the microearthquakes that occurred in Irpinia with local magnitude (ML) ranging between 0.1 and 3.7.

This discrepancy between time-domain and frequency-domain estimates of the stress release has been already pointed out by Boatwright (1984), where it was showed that frequency-domain (Brune, 1970) stress-drop is best-correlated with dynamic stress and uncorrelated with static values, better represented by time-domain estimations of the source radius.

The discrepancy between the stress-drop values obtained from this method and the frequency techniques is also observed by Zollo et al. (2021) for the moderate to large magnitude events. However, it is a more problematic issue for the micro-events, that source duration is at the same level or smaller than the time sample rate of the recorded seismograms and precise measurement of the corner time is not an easy task. In fact, any small error in corner time estimation caused a large error in the stress-drop calculation as these two parameters are correlated with inverse quadratic relation (equation (5)). Nevertheless, Fig. 4e and f obviously show that our results assuming both approaches are consistent with each other. Also, it is worth noting that the spectrum methods are model-dependent by themselves and choosing the Brune (1970) or Madariaga (1976) models could result in different values of earthquake source parameters.

5. Conclusions

In this paper, we have presented a flexible MATLAB package with the

aim of rapid and automatic determination of the earthquake source parameters such as seismic moment (M_0), duration of the rupture, fault geometry, and static stress drop, which is recently developed by Zollo et al. (2021). This package is well suited to be modified for more complex modeling if desired. For example, it can be altered for use of the S-wave instead of the P-wave content. The same approach could be also adapted for the real-time estimation of the source parameters. The time-domain technique implemented in this package could be used as an alternative or complement the well-known standard spectral techniques for the characterization of the earthquake source.

Code availability section

Name of the code/library: EASOt-Ap.

Contact: nazeri.sahar@gmail.com.

Program language: MATLAB (R2021a)

Source code: <https://github.com/SaharNazeri/EASOt-AP>.

Authorship contribution statement

Sahar Nazeri: Data curation, Formal Analysis, Software, Methodology, Visualization, Writing Original Draft, Review and Editing. Aldo Zollo: Conceptualization, Methodology, Validation, Writing Original Draft, Review and Editing, Supervision, Funding Acquisition.

Declaration of competing interest

The authors declare that they have no known competing financial interests or personal relationships that could have appeared to influence the work reported in this paper.

Data availability

Data will be made available on request.

Acknowledgments

We would like to acknowledge the Irpinia Seismic Network (ISNet) and RISSCLab team for managing the data collection and distribution. This work has been partially funded by the Project PRINFLUID, financed by the Italian Ministry of Research. The authors would like also to express their appreciation to Luca Elia (Naples Federico II university, Italy) for his constructive assistance.

Appendix

Description of the inputs and the default values of the “Input” file.

- (1) “Region”: name of the studied area, same as the name of the main directory of data i.e., (Package/INPUT/“Region”). Inside this folder, SAC files of all events are presented in separate subfolders for each event that can be specified with any kind of name, for example date and time of the occurrence of the event. After running the package, a directory with the same name of the region will be created automatically inside the folder of the “OUTPUT” as (Package/OUTPUT/“Region”).
- (2) “wave-type”: type of the raw ground motion data as “A” (Acceleration) or “V” (Velocity). (Default: A).
- (3) “dirparam”: specific part of the name of the SAC-formatted waveforms to make directory. (Default: *sac*).
- (4) “CF, Unit”: CF is a conversion factor to change the conventional unit of amplitude to the SI unit i.e., m/s² or m/s for acceleration or velocity respectively. “Unit” can be set as Yes or No depends on existence of a unique CF value for whole data or not. In the case of setting “Unit” as “No”, different conversion factors corresponding to each waveform will be read from the header of the SAC formatted data stored as the “scale” field. (Default: 1, No).
- (5) “minSta”: minimum number of stations required to make average and build up the LPDT curve at each time sample. (Default: 5)
- (6) “Rmax”: maximum hypocentral distance in km to select data within, for events with different range of Magnitude: M ≤ 1, 1 < M ≤ 3, 3 < M ≤ 5, and M > 5. (Default: 20, 40, 60, 100).
- (7) “SNR”, the threshold value for SNR to exclude the bad quality signals. (Default: 10).
- (8) “nPol, cor1, cor2”: number of poles (nPol) and two corner frequencies (cor1, cor2 in Hz) of the band-pass Butterworth filter applied to the displacement. (Default: 2, 1, 30).
- (9) “Vfilter, nPolV, cor1V, cor2V”: number of poles (nPolV) and two corner frequencies (cor1V, cor2V in Hz) of the band-pass Butterworth filter applied to the velocity signals in case that “Vfilter” is set as “Yes”. If “Vfilter” is assigned as “No”, no filter is applied to the velocity waveforms. In the other words, this step is optional based on the “Vfilter” value. (Default: No, 2, 0.075, 30).
- (10) “WinFix, WinMax, S_P_Coeff”: the P-waves are windowed after the onset using a fix (WinMax) or variable values for each station, depending on what is set as the “WinFix”, i.e., “Yes” or “No” respectively. In case of selecting the variable time window, the S-mines-P coefficient (S_P_Coeff) is then used to calculate the length of the window from the P-wave to the S-wave. (Default: No, 1, 0.09).
- (11) “WinFix_fit, WinMax_fit”: selecting a fix time window (WinFix_fit set as “Yes”) to fit to the LPDT curve with length of “WinMax_fit”. If “WinFix_fit” is assigned as “No”, the entire of the LPDT curve is used to find the best nonlinear fit to the curve. (Default: No, 1).
- (12) “rho, Vp, Vs, SD”: properties of the medium i.e., density of the area (rho in kg/m³), P-wave velocity (Vp in m/s), S-wave velocity

(Vs in m/s), and trial value of Stress Drop (SD in MPa). (Default: 2700, 5500, 3000, 1)

- (13) “RadP”: P-wave radiation pattern coefficient. (Default: 0.52).
- (14) “QFilter, Qp”: implementing (on) or ignoring (off) the anelastic attenuation analysis. In case of implementing this correction, the constant Qp-value for the studied area is assumed to remove the anelastic attenuation from the final solution of STF. (Default: on, 150).
- (15) “FitFun”, selecting the fit function to model the LPDT curve, among two options of “exp” or “HB”, (see section C. Modelling the LPDT curve and Table 1 for more detail). (Default: “HB”).
- (16) “SD1, SD2, SDN”: range of the static stress drop in MPa from SD1 to SD2 which this interval is divided to SDN values to find the best stress drop value implementing the “Approach 1”.

References

- Aki, K., 1966. Generation and propagation of G waves from the Niigata earthquake of June 16, 1964: Part 2. Estimation of earthquake moment, released energy and stress drop from the G wave spectra. Bull. Earthq. Res. Inst., Univ. Tokyo 44, 73–88.
- Aki, K., Richards, P.G., 2002. Quantitative Seismology. University Science Books, Sausalito, CA.
- Amoroso, O., Ascione, A., Mazzoli, S., Virieux, J., Zollo, A., 2014. Seismic imaging of a fluid storage in the actively extending Apennine Mountain belt, southern Italy. Geophys. Res. Lett. 41, 3802–3809. <https://doi.org/10.1002/2014gl060070>.
- Boatwright, J., 1984. Seismic estimates of stress release. J. Geophys. Res. 89, 6961–6968. <https://doi.org/10.1029/JB089iB08p06961>.
- Brune, J.N., 1970. Tectonic stress and the spectra of seismic shear waves from earthquakes. J. Geophys. Res. 75, 4997–5009. <https://doi.org/10.1029/jb075i026p04997>.
- Colombelli, S., Zollo, A., Festa, G., Picozzi, M., 2014. Evidence for a difference in rupture initiation between small and large earthquakes. Nat. Commun. 5, 3958.
- CREWES, 2020. Abstract book. CREWES Research Report 32, 86.
- Festa, G., Adinolfi, G.M., Caruso, A., Colombelli, S., De Landro, G., Elia, L., Emolo, A., Picozzi, M., Scala, A., Carotenuto, F., et al., 2021. Insights into mechanical properties of the 1980 Irpinia fault system from the analysis of a seismic sequence. Geosciences 11, 28. <https://doi.org/10.3390/geosciences11010028>.
- Hanks, T.C., Kanamori, H., 1979. A moment magnitude scale. J. Geophys. Res. 84 (B5), 2348–2350.
- Keilis-Borok, V., 1959. On estimation of the displacement in an earthquake source and of source dimensions. Ann. Geofisc. 12, 205–214. <https://doi.org/10.4401/ag-5718>.
- Kjartansson, E., 1979. Constant Q-wave propagation and attenuation. J. Geophys. Res. 84, 4737–4748.
- Madariaga, R., 1976. Dynamics of an expanding circular fault. Bull. Seismol. Soc. Am. 66 (3), 639–666.
- Mjaavatten, A., 2022. Curvature of a 1D curve in a 2D or 3D space (MATLAB Central File Exchange). <https://www.mathworks.com/matlabcentral/fileexchange/69452-curvature-of-a-1d-curve-in-a-2d-or-3d-space>.
- Nazeri, S., Shomali, Z.H., Colombelli, S., Elia, L., Zollo, A., 2017. Magnitude estimation based on integrated amplitude and frequency content of the initial P wave in earthquake early warning applied to Tehran, Iran. Bull. Seismol. Soc. Am. 107 (3), 1432–1438. <https://doi.org/10.1785/0120160380>.
- Nazeri, S., Colombelli, S., Zollo, A., 2019. Fast and accurate determination of earthquake moment, rupture length and stress release for the 2016–2017 Central Italy seismic sequence. Geophys. J. Int. 217 (2), 1425–1432. <https://doi.org/10.1093/gji/ggj097>.
- Wang, Y., Colombelli, S., Zollo, A., Song, J., Li, S., 2021. Source parameters of moderate-to-large Chinese earthquakes from the time evolution of P-wave peak displacement on strong motion recordings. Front. Earth Sci. <https://doi.org/10.3389/feart.2021.616229>.
- Zollo, A., Nazeri, S., Colombelli, S., 2021. Earthquake seismic moment, rupture radius, and stress drop from P-wave displacement amplitude versus time curves. IEEE Trans. Geosci. Rem. Sens. 60, 1–11. <https://doi.org/10.1109/TGRS.2021.3119909>, 2022, Art no. 5912211.
- Zollo, A., Lancieri, M., Nielsen, S., 2006. Earthquake magnitude estimation from peak amplitudes of very early seismic signals on strong motion records. Geophys. Res. Lett. 33, L23312 <https://doi.org/10.1029/2006GL027795>.
- Zollo, A., Orefice, A., Convertito, V., 2014. Source parameter scaling and radiation efficiency of microearthquakes along the Irpinia fault zone in southern Apennines, Italy. J. Geophys. Res. Solid Earth 119, 3256–3275. <https://doi.org/10.1002/2013jb010116>.